Multiple-ionization collision dynamics

R. E. Olson

Gesellschaft für Schwerionenforschung, D-6100 Darmstadt, Federal Republic of Germany
and Department of Physics, University of Missouri–Rolla, Rolla, Missouri 65401

J. Ullrich and H. Schmidt-Böcking

Institut für Kernphysik, Universität Frankfurt, D-6000 Frankfurt am Main, Federal Republic of Germany
(Received 30 December 1988)

The 1.4-MeV/u U^{32+} + Ne collision system is studied in detail in order to elucidate the dynamics of multiple ionization in energetic, heavy-ion–atom collisions. Differential cross sections versus recoil-ion charge state, calculated by the n-body classical-trajectory Monte Carlo method, are presented for the θ and φ angle dependences of the projectile, recoil ion, and ejected electrons. The calculations show a high degree of ejected-electron asymmetry towards the projectile side of the target nucleus which strongly effects the transverse-momentum balance between the heavy particles. Experimental and calculated cross sections differential in the recoil-ion charge state and transverse momentum are found to differ by orders of magnitude from those for the projectile, providing evidence for the importance of explicitly considering the ejected electrons' momenta in the determination of the heavy-particle (both the projectile and the recoil-ion) angular differential cross sections. Polarization of the target electrons and screening of the recoil ion by the ejected electrons lead to $\sim 10^{-6}$-rad negative-angle deflections of the projectile for recoil-ion charge states up to 4+. The angular scattering of the recoil ion departs significantly from that predicted for a two-body collision, and is found to be nearly isotropic for low recoil-ion charge states and peaked to angles $\theta > 90°$ for high recoil-ion charge states. A stopping-power calculation for this system is in good agreement with the experimental value. Stopping powers differential in impact parameter and for energy deposition to δ electrons and multiple ionization are given to further describe the projectile energy loss.

INTRODUCTION

A detailed understanding of multiple-ionization and electron-capture mechanisms in energetic ($\sim$MeV/u) collisions between multiply charged ions and atoms is a difficult task, due to the many-body nature of the interaction. For a representative system of the form

$$A^{q+} + B \rightarrow A^{(q-j)+} + B^{i+} + (i-j)e^- , \qquad (1)$$
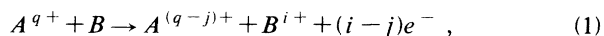
it is essential that studies simultaneously investigate the cross sections for producing various recoil-ion charge states, B^{i+}, the change in charge of the projectile ion $(q-j)+$, and the spectra of the ejected δ electrons $(i-j)e^-$.

Experimentally, rapid progress has been made in the last 15 years. Early on, observations[1,2] of Doppler broadening from the radiation emitted from the recoil ions implied that these ions were produced with low kinetic energies, $E \leq 10$ eV, even though the collision system possessed hundreds of MeV of kinetic energy. In 1979, Cocke[3] presented total ionization cross sections differential in the recoil-ion charge state, from the magnitude of which, one could deduce the long-range nature of the collisions such as (1). Shortly thereafter, total net ionization cross-section measurements were made for a large variety of projectiles and gas targets, and a scaling rule was developed to predict cross sections for other systems.[4] Measurements, differential in recoil-ion and final-

projectile-ion charge states, were undertaken by several groups.[5–7] Very recently, direct measurements[8–10] have been made for the translational energy of B^{i+}. Also, projectile angular scattering and energy loss have been investigated using sophisticated experimental techniques.[11,12] Furthermore, δ-electron spectra have recently been reported for U^{q+} projectiles over a wide range of electron energies and ejection angles.[13]

Theoretically, the study of reaction (1) is complicated by the fact that over a large impact-parameter range the number of electrons participating in the collision equals that of the target atom. Thus, the many-body Coulomb interaction must explicitly be solved. Therefore, in general, theoretical developments have lagged behind experimental ones. Early calculations employed classical models[14] and the semiclassical approximation.[15] Later on, another set of calculations[16] used the hydrogenic, three-body classical-trajectory Monte Carlo (CTMC) method[17] along with the independent-particle model (IPM) which essentially reduces the many-body interaction to a single-electron problem.[18,19] Another set[3] used an energy-deposition model originally developed by Russek and Meli[20] to analyze the experiments of Everhart and Kessel.[21,22] The IPM method has been central to several CTMC calculations using hydrogenic atoms,[23] and to similar ones based on a Thomas-Fermi description of the target atom.[24] Even with the inclusion of shell structure on the target atom, the calculations became increasingly inaccurate for the prediction of ionization cross sections

for highly charged recoil ions.[6] The difficulty does not lie with the assumption of a Hartree-type product wave function. The problem appears to lie with the single-electron approximation used to model the outer electron shells active in the collision. For these shells, the binding energy varies rapidly with the recoil-ion charge state, and the IPM does not reproduce the correct energy deposition. Corrections for this deficiency have been introduced by Horbatsch using a time-dependent target-atom screening which has been normalized to experimental data.[25]

Recently, we have used a new approach which exploits advances in vector-processing computer technology. We have termed it the n-body classical-trajectory Monte Carlo (nCTMC) method and explicitly include all electrons in the calculations[9,23] The method is constructed to account for the correct energy deposition per stage of target ionization. It allows, for the first time, the prediction and comparison with experiment as to the angles and energies of the projectile and recoil ion without making any assumption about scattering potentials other than pair-wise Coulomb interactions. Dynamical polarization of the target atom, post-collision interactions of the electrons with the projectile and recoil ion, are inherently included in the calculations and are a natural evolution of the Coulomb forces between the particles.

In this paper, we present calculated cross sections differential in recoil-ion charge state for the angular scattering (in both θ and azimuthal (φ) planes) of the projectile and recoil ion. Electron spectra are also given along with a comparison with stopping-power (energy-deposition) measurements. Experimental transverse-momentum spectra of the recoil ion, differential in the recoil-ion charge state, are compared with the nCTMC calculations. From these comparisons, conclusive evidence is given as to the importance of the δ electrons in the transverse-momentum balance. Asymmetry in the δ-electron emission leads to large differences in the transverse momenta carried away by the projectile and recoil ions after the collision. Orders-of-magnitude differences are predicted for these respective cross sections.

We have concentrated on the 1.4-MeV/u $U^{32+}+Ne$ system due to the availability of detailed cross-section measurements. The laboratory coordinate system is used for the differential-cross-section examples.

THEORY

A theoretical treatment of the many-body reaction (1) is faced with the need to make approximations that do not cloud an interpretation and prediction of the collisional behavior. Several different theoretical approaches can be applied, each of which has its own attributes and limitations. Perturbation methods appear to be particularly inappropriate, since the system is strongly coupled. The transition probabilities approach unity even at intermediate values for the impact parameter.

A quantum-mechanical approach would be most desirable. However, limitations as to basis-set size make it very difficult to encompass excitation, electron capture, and electron ionization in the strong transient fields of

the highly charged projectile and recoil ion. A further difficulty is the basis-set representation of the continuum levels associated with multiple ionization. Furthermore, the separation between electronic and nuclear motion used in present quantum-mechanical treatments does not allow for a direct prediction of the angular scattering of the heavy particles. Arbitrarily assumed scattering potentials, such as screened Coulomb or Thomas-Fermi interactions, must be utilized in order to estimate the angular deflections. In this paper, we will demonstrate that this latter step is complicated, and in many cases invalidated, by the anisotropic emission of the ionized electrons.

The use of the independent-particle model[18,19] with transition probabilities determined within a single-electron calculation has appealing features. The transition probabilities may be calculated using standard classical, semiclassical, or quantum-mechanical methods. The IPM preserves unitarity in the scattering transition probabilities, can encompass electron-shell effects, and is easy to use. This method is especially applicable to inner-shell processes where a single-electron approximation can usually adequately represent a given electron shell. For outer-shell processes, such as in (1), the method does not reproduce the energy deposition required to follow various degrees of ionization. As for quantal treatments, angular scattering of the heavy particles does not naturally evolve from this theoretical method.

In order to circumvent many of the above theoretical difficulties, we have developed an n-body classical-trajectory Monte Carlo (nCTMC) method that directly includes all target electrons in the calculations.[9,23] The classical treatment is designed to reproduce the quantum-mechanical hydrogenic momentum distributions for the electrons, and uses spectroscopic energy levels to determine the initial electron distributions. All interactions of the projectile and the target nuclei with each other and the electrons are explicitly included in the calculations. This allows a direct determination of the angular scattering for the particles after the collision, along with an estimate of the energy deposition to the electrons and the heavy particles. The classical determination of the angular scattering is strengthened by the equivalence in Rutherford scattering between point charges within both classical and quantum-mechanical methods. For this system, the uncertainty principle applies only to $\theta \le 10^{-7}$ rad.

The nCTMC method has the equivalent of an infinite basis set which easily spans the ionization continuum. However, quantized levels are used for the initial electron distributions, but quantization is not preserved after the collision. Furthermore, although post-collision interactions are included between the projectile and recoil ions with the electrons, electron-electron interactions are introduced only in the bound initial states via screening factors in a central-field approximation. One may argue that electron-electron correlation interactions are of minor importance here, due to the large disparity in charge between the electrons and the projectile. However, important effects may be ignored,[26] as has been seen by the need to include electron-electron interactions to

accurately describe double ionization of helium by protons and antiprotons.[27,28]

The nCTMC calculations require the numerical integration of several thousand trajectories so that a microcanonical distribution of electron orbits may be realized. We have assumed the projectile electrons to be inert in the calculations, and have simply used a point charge for the U^{32+} ion. Such an approximation appeared reasonable since the present experiments demonstrated that stripping in coincidence with recoil-ion production was below observable levels.

The Hamiltonian for reaction (1) has been written as

$$H = p_a^2/2m_a + p_b^2/2m_b + \sum_{i=1}^{N} (p_i^2/2m_e + Z_a Z_i/R_{ai}$$

$$+ Z_b Z_i/R_{bi}) + Z_a Z_b/R_{ab}, \qquad (2)$$

where N is the number of electrons on target atom B, and the indices a and b represent the projectile ion and target nucleus, respectively. From Eq. (2), one obtains a set of $6(N+2)$-coupled, first-order differential equations arising from the necessity to determine the time evolution of the xyz Cartesian coordinates of each particle,

$$\frac{dc_j}{dt} = \frac{\partial H}{\partial p_j}, \qquad (3)$$

and their xyz momenta

$$\frac{dp_j}{dt} = -\frac{\partial H}{\partial c_j}. \qquad (4)$$

The electrons are initially placed in a microcanonical distribution of orbits about the target nucleus with an effective-interaction charge $Z_b Z_i$, determined by the sequential ionization energies U_i of the target electrons

$$Z_b Z_i = n_i |2U_i|^{1/2}. \qquad (5)$$

The $6(N+2)$-coupled equations are solved numerically using a variable-step Runge-Kutta-Gill method for a randomly determined distribution of electron orbits and impact parameters.

In practice, we routinely need about 5000 different trajectories to obtain the total cross sections for reaction (1). Cross sections differential in angle or energy require several tens of thousand trajectories. Hence, the method requires computer time equivalent to the molecular- or atomic-orbital scattering calculations used at lower energies.

After the collision, it is possible to compute the electronic energy of the residue target ion and that of the projectile after electron capture. In the event that an electron is captured by the projectile, a classical-product n level is assigned according to the hydrogenic formula

$$n_c = q/|2U|^{1/2}, \qquad (6)$$

where q is the charge of the incident ion and U is the electronic binding energy. Becker and MacKellar[29] have used a principle of proportionality of classical and quantal weights in order to identify quantal-product n levels

from the classical values determined by Eq. (6). By requiring that the phase space per bin be equal to the quantal n^2 multiplicity of a given level n, they have shown that the relation

$$[(n-1)(n-\tfrac{1}{2})n]^{1/3} \le n_c \le [n(n+\tfrac{1}{2})(n+1)]^{1/3} \qquad (7)$$

determines the correspondence between classical and quantal n levels. Numerous CTMC calculations[30] have employed Eqs. (6) and (7) to determine electron-capture n levels for multiply charged ions colliding with hydrogenic atoms. For these cases, the classical results reproduce available experimental observation.[31]

The electronic excitation of the recoil ion is also monitored after the collision, in order to account for Auger events and the indistinguishability of the electrons. The extent of electronic excitation can be determined by comparing the calculated total electronic energy against spectroscopic values for the various recoil-ion charge states. If multiple excitation is found to have left the ion in a continuum state, we have assumed an 100% Auger-to-radiative decay branching leading to autoionization. Such an assumption is crude but sufficiently accurate for these scattering calculations, particularly when a given electron shell is in its early to middle stages of ionization. The inclusion of post-collision autoionization has been found to be very important at high energies, $E \ge 100$ MeV/u, where we have shown that the total ionization cross sections will be increased by up to a factor of 8 over the direct collisional-ionization values.[32] For the 1.4-MeV/u U^{32+} + Ne system under study here, we find an average increase of ~65% in the total ionization cross sections. This increase is primarily due to contributions from multiple excitation at larger impact parameters than that for the direct-ionization component.

EXPERIMENT

As has been reported in detail,[33,34] we have developed an experimental time-of-flight (TOF) technique, which allows the simultaneous determination of the charge state i and the transverse (with respect to the beam axis) momentum $p_\perp$ of the recoiling target atom, in coincidence with the charge-state-analyzed outgoing projectile. Applying this technique, $p_\perp/p_\parallel$-dependent cross sections ($p_\parallel$ is the incoming projectile momentum) for different final projectile and recoil-ion charge states could be obtained for the collision system under consideration. Since the precision achieved in the determination of $p_\perp$ is comparable to a microradian θ measurement, the multiple-ionization process could be investigated very sensitively in the large-impact-parameter regime which makes a maximum contribution to the multiple-ionization cross sections.

The experiment was performed at the UNILAC accelerator of Gesellschaft für Schwerionenforschung GSI, Darmstadt ("Stripperhalle"). The charge-state-analyzed uranium beam is collimated to a beam spot of less than 0.2 mm diameter by three collimators. The last one of them is located directly in front of the time-of-flight spectrometer (TOFS) to provide a well-defined beam trajecto-

ry inside the apparatus. Having passed the scattering region in the TOFS, the projectiles were charge-state analyzed by a magnetic field and detected in a position-sensitive parallel-plate avalanche detector. The gas target pressure inside the innermost cylinder (target region) of the TOFS was about 10^{-4} Torr and low enough to ensure single-collision conditions. The produced recoil ions drift towards the walls of the inner cylinder of the TOFS (diameter; 5 mm) according to the velocity $v_\perp$ transferred from the projectile's kinetic energy. A small fraction of these ions leave the target cell through an opening of 1 mm diameter (solid angle in the azimuthal plane $\Delta\varphi/2\pi = 3\%$, where φ is the azimuthal angle). They are then accelerated in an electric field, applied between an inner and outer cylinder (≈ 320 V/cm), focused by an einzel lens, charge-state analyzed in the variable field of two ajustable permanent magnets, and finally detected by a two-dimensional position-sensitive channel-plate detector system. A coincidence between the delayed signal of the projectiles and the time signal of the recoil ions provides time-of-flight spectra for specific $(q-j,i)$ channels, where $q-j$ is the final charge state of the projectile and i is that of the recoil ion. Since the target region is free of electric fields, the measured TOF is directly related to the velocity the recoil ions gain during the encounter. The obtained spectra have to be corrected for the flight times of the projectiles and the recoil ions in the detection branches of the apparatus to obtain the time of flight the recoil ions need to traverse the radius of the inner cylinder.

After subtraction of background events, the TOF spectra were transformed into $p_\perp/p_\parallel$-dependent distributions to compare with theoretical calculations. Absolute experimental cross sections were obtained from the pressure dependence of charge-exchanged fractions of the incoming beam, determined in a separate experiment (for details of the data analysis, the normalization procedure and the discussion of experimental errors, see Refs. 35 and 36). The experimental data presented are differential in the charge state and in the relative momentum of the recoil ions, but integrated over the final charge states of the projectile (ionization plus capture).

The experimental data in Ref. 35 excluded capture channels of the projectile, and the absolute normalization was based on the theoretical results of Horbatsch.[37] In this work, the normalization is based on new experimental measurements. Furthermore, the $p_\perp/p_\parallel$ scale given here is shifted by $+1.2\times10^{-6}$ compared to previous results; the experimental error in the $p_\perp/p_\parallel$ scale now is $\pm1.2\times10^{-6}$ instead of $+2.4\times10^{-6}$ ($+20$ meV) stated before. For these reasons, minor differences between previously published experimental data and those presented in this paper can be observed concerning the magnitude (absolute normalization) and the shape (inclusion of capture channels) of the data.

Due to the new insight in the collision dynamics presented in this paper, there is strong evidence that the transverse momenta of the projectile and the recoil ion are not equal, and therefore the θ scale given in the previous publications should be replaced by the experimentally determined quantity, namely, $p_\perp/p_\parallel$.

RESULTS

Total cross sections

The calculated total cross sections for ionization and electron capture are shown in Fig. 1 as a function of the charge state of the recoil ion. Experimental cross sections have been measured for the ionization and the single-electron-capture processes. Both the calculated and experimental values are absolute, and have not been normalized to other work. In general, we find qualitative agreement between theory and experiment. Exceptions are in the position of the single-electron-capture which is located at Ne^{5+} experimentally, while the calculations yield Ne^{7+}. Another difference is that at high recoil-ion charge states, $i \geq 8$, the calculated ionization cross sections lie below the electron-capture values, while the opposite is true for the experimental results. Such a trend indicates that the "true" electron-capture transition probabilities are of longer range than predicted by the nCTMC method. Autoionization of the excited target atom after the collision has been included in the theoretical calculation. Tests were made to assure single-collision conditions; however, it is possible that there may have been stripping of projectiles that captured electrons into high n levels. This effect would enhance the experimental ionization cross sections at the expense of the electron-capture ones.
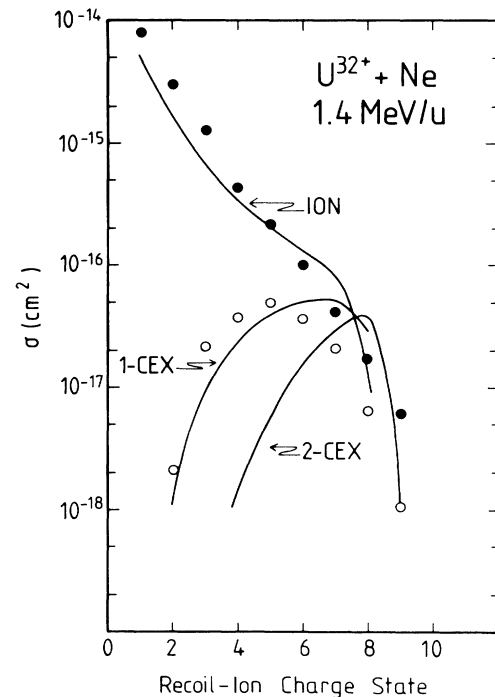

FIG. 1. Total cross sections for ionization (ION), and single (1-CEX) and double (2-CEX) electron capture as a function of Ne^{i+} recoil-ion charge state. The lines are nCTMC results and the symbols are experimental values for ionization (solid circles) and single-electron capture (open circles).

The integral cross sections, summed over all recoil-ion charge states, have been measured by us for this system. Here, the agreement is quite good between theory and experiment. Cross-section values are the following: ionization, 8.0×10^{-15} cm^2 versus 1.3×10^{-14} cm^2; single-electron capture, 2.0×10^{-16} cm^2 versus 1.8×10^{-16} cm^2; and double-electron capture, 9.1×10^{-17} cm^2 versus 5.5×10^{-17} cm^2, for theory and experiment, respectively. The experimental integral cross sections are estimated to be accurate to $\pm 30\%$.

The long-range nature of the ionizing collisions is exemplified by the magnitude of the cross sections which considerably exceed 10^{-15} cm^2 for low recoil-ion charge-state production. An examination of the transition probabilities (Fig. 2) for electron removal (ionization plus electron capture) reveals significant transition probabilities at impact parameters $b \gtrsim 10a_0$. In fact, the transition probabilities do not decrease below 1% until $b \gtrsim 18a_0$. Furthermore, the sum of the transition probabilities for electron removal exceeds 50% for $b \leq 9a_0$, indicating the extremely strong coupling in such collisions. Noteworthy is the fact that the electron-removal probabilities for recoil-ion charge states $i \geq 7$ maximize at impact parameters greater than the L-shell radius of the Ne atom. Thus penetration of the target's electron cloud by the projectile is not required to realize a high stage of ionization.

From the calculations, it is also possible to predict the n principal quantum number of the captured electron. Single-electron-capture results are shown in Fig. 3. The hydrogenic model described in a previous section has been used for the calculations. Hence there may be shifts in the values when the closed shells of U^{32+} and the quantum defects of the excited levels are considered in detail. The electron capture is found to be broadly distributed with a maximum at $n \approx 7$ or 8. For large n values, we find the nCTMC values closely follow the expected n^{-3} scaling.
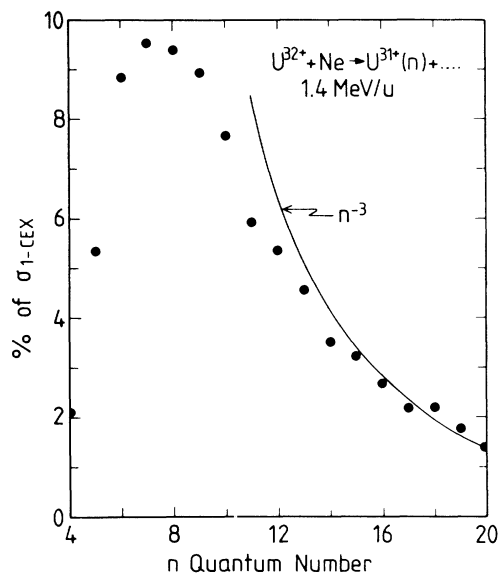
FIG. 3. Calculated n principal-quantum-number distributions for single-electron capture (solid circles). A $1/n^3$ functional form is also shown.

There is considerable electron capture to high-lying Rydberg levels. In fact, the calculations indicate that $\sim 48\%$ of the single-electron capture proceeds to $n > 10$. Such behavior is consistent with projectile equilibrium charge-state distributions observed for U^{q+} ions in gases and solids. In a gas, the ion has sufficient time to radiatively decay after electron capture, before the possibility of being stripped in a subsequent collision presents itself. In a solid, the electrons captured to high-lying states are stripped with high probability in a collision time short compared to the radiative decay time. The n-state distributions shown in Fig. 3 are consistent with observations that the equilibrium charge state for 1.4-MeV/u U^{q+} maximizes at $q \approx 29$ for gases and $q \approx 41$ for solids.[38]

Since the energies of the product collision particles can be calculated using the nCTMC method, it is possible to present the calculated energy deposition, in the laboratory frame, as a function of recoil-ion charge state (Table I). As has been already discussed,[9] the energy carried away by the Ne^{i+} recoil ion is a negligible component of the projectile energy of 1.4 MeV/u$=333$ MeV available to the various products. The recoil-ion energies are generally found to be less than 1 eV. The average energy per ejected δ electron (note, the table does not include the captured electrons) is found to increase significantly with recoil-ion charge state or decreasing impact parameter (see Fig. 2). The projectile's average energy loss is on the order of several keV, and also increases with the violence of the collision at small impact parameters. Measured values for the 0.83-MeV/u C^{6+}+Ne system are consistent with the nCTMC calculations.[11] For reference, the right-hand column of Table I gives the sequential ionization energy required to remove i electrons from Ne to the continuum with zero translational energy.
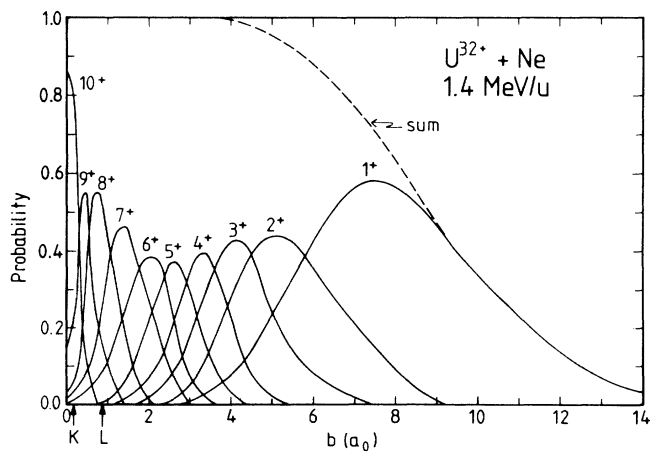

FIG. 2. Calculated transition probabilities for electron loss (sum of ionization and electron capture) as a function of Ne^{i+} recoil-ion charge state. The expectation values for the radii of the K and L shells of the Ne atom are noted along with the sum of the recoil-ion charge-state-dependent transition probabilities.

TABLE I. Energy deposition in the 1.4-MeV/u U^{32+} + Ne collision.

Recoil-ion charge state i	Average recoil-ion energy (eV)	Average energy per δ electron (eV)	Average projectile energy loss (eV)	Ionization energy (eV)
1	0.049	26	72	22
2	0.051	63	240	63
3	0.053	110	540	130
4	0.072	190	1200	220
5	0.12	270	2000	350
6	0.24	360	3200	510
7	0.70	500	4900	710
8	2.8	630	7000	950

Differential cross sections of the ionized electrons

It is of interest to examine the energy and angular dependence of the ionized electrons for reaction (1). These secondary electrons make important contributions to far-ranging damage in biological cells and semiconductor devices when a high-Z energetic ion passes through them.

The calculated energy spectrum, integrated over all emission angles, for the ionized electrons is shown in Fig. 4. It is highly peaked towards low electron energies, which reflects the "soft" large-impact-parameter collisions that dominate the ionization cross sections. The nCTMC values are consistent with the measurements of Kelbch et al.,[13] also shown in Fig. 4, which are available for ejected-electron energies from 200 to 750 eV.

The angular dependence integrated over all electron energies of the ionized electrons is given in Fig. 5. The singly differential cross sections have an almost constant value until 90°, beyond which they decrease rapidly. It

should be noted that this spectrum is dominated by slow electrons, see Fig. 4, which are removed by large-impact-parameter collisions. In these cases, the electrons are preferentially attracted toward the highly charged ion at the distance of closest approach.

Cross sections doubly differential in angle and energy allow the collision dynamics to be more fully revealed. In Fig. 6 are given the angular distributions for electrons ejected with energies 50±50 eV, 500±50 eV, and 1000±100 eV. The symbol designated BP refers to binary peak electrons which arise from an assumed two-body collision between the projectile and a "free" electron. For a given ejected electron velocity, the binary peak is determined from

$$\theta_{BP} = \cos^{-1}[v_e/(2v_p)] , \qquad (8)$$

where v_e and v_p are the velocities of the electron and projectile, respectively.

The cross sections are found to decrease rapidly at angles greater than the binary peak. For the 50-eV electrons, this behavior is not as pronounced as at the higher energies due to the relatively large acceptance-energy window used in the calculations. The slow electrons appear to be nearly equally scattered for $\theta \leq \theta_{BP}$ due to the
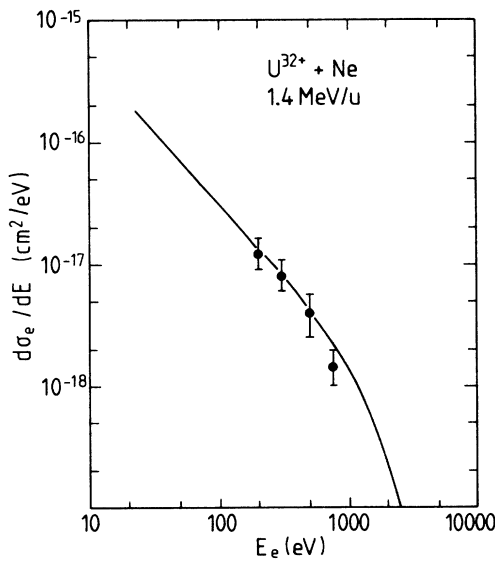

FIG. 4. Ionized-electron spectrum differential in energy. The closed circles are experimental data (Ref. 13) and the line is the nCTMC result.
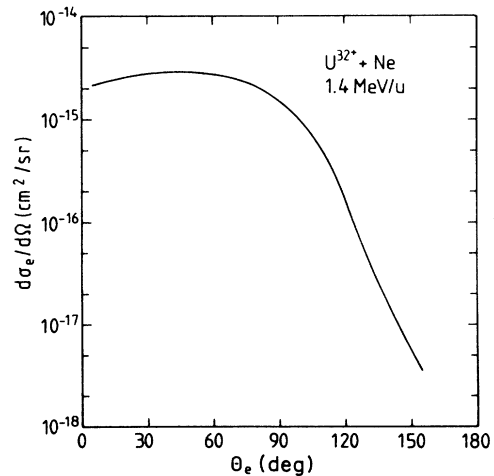

FIG. 5. Ionized-electron spectrum differential in angle from nCTMC calculations.
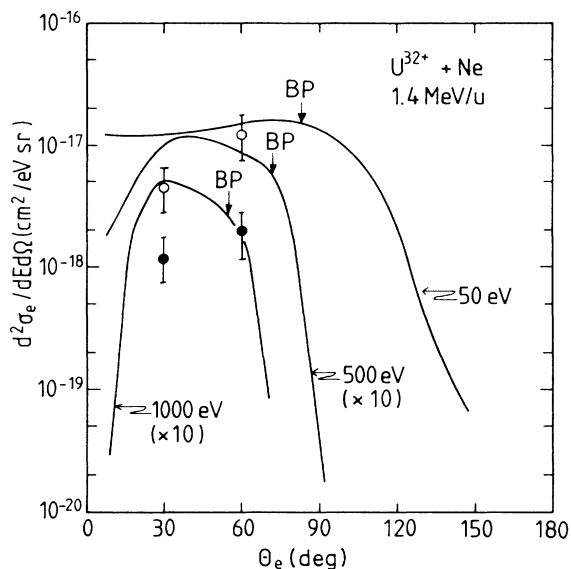
FIG. 6. Ionized-electron spectra differential in energy and angle. The position of the binary peak (BP) is noted on each curve. The lines denote nCTMC results for ionized electron energies of 50 ± 50 eV, 500 ± 50 eV, and 1000 ± 100 eV. Experimental data from Kelbch et al. (Ref. 13) are given for 500 eV (open circles) and 1000 eV (closed circles).

importance of two-center effects in the electron spectra. However, the fast electrons appear to be "focused" on angles slightly smaller than the binary peak, and also display small cross sections near 0°. The peak is broadened because the electrons have initial momentum distributions before the collision that are associated with their bound electronic levels and are distorted by the recoil ion's Coulomb potential during the ionizing collision.

Experimental values from Kelbch et al.[13] are available for 500-eV ionized electrons (open symbols in Fig. 6) and for 1000-eV electrons (closed symbols). Considering the highly differential nature of the calculations and experiment, the agreement could be considered fair. Although there is agreement to a factor of 3 in absolute magnitude, the experiments indicate that the cross sections may be more highly peaked near θ_{BP}. However, similar measurements and calculations for the 1.4-MeV/u $U^{32+}+Ar$ system do not display such a large discrepancy in shape.[13]

Heavy-particle angular scattering

The angular scattering of an energetic heavy ion such as 1.4-MeV/u U^{32+} in an ionizing collision with a rare-gas atom is very difficult to attain experimentally. This is because the angular deflections are $\lesssim10^{-5}$ rad, which amounts to a 1-cm deflection in 1 km. Because of this severe constraint, we[33,34] have designed and built a recoil-ion detector which measures the transverse momentum spectra of the recoil ions along with their charge states. In principle, if the summed momentum vectors of the electrons equal zero or are very small compared to that for the heavy particles, the transverse momentum of the recoil ion will equal that of the projectile ion, and a division by the projectile's initial momen-

tum will yield the scattering angle.

In the nCTMC calculations, it is not necessary to assume isotropic electron emission and the equivalence in the magnitude of the transverse momenta for the recoil and projectile ions. In fact, deviations from this expected behavior will clearly signal the importance of the ejected electrons in the transverse-momentum balance of the heavy particles.

A direct comparison between experimental and calculated recoil-ion momentum spectra is possible. In Fig. 7 are shown the calculated and experimental values for the transverse-momentum spectra of all recoil ions produced in reaction (1)—solid line and closed symbols, respectively. Measurements and calculations that are in coincidence with electron capture by the projectile are given by the open symbols and dashed line, respectively. The calculated values have been folded with the Boltzmann temperature distribution in the gas target cell. The inclusion of the Boltzmann distribution only effects values of $p_\perp/p_\parallel \lesssim5\times10^{-6}$. In general, there is good agreement between theory and experiment, not only in absolute magnitude but also in the shape of the cross sections. However, there is a tendency for the theory to overestimate the small-impact-parameter collisions, which shows itself at high transverse momenta $p_\perp/p_\parallel \gtrsim2\times10^{-5}$ and in the total-cross-section differences for high recoil-ion charge-state production, Fig. 1.

To further illuminate the comparisons, it is possible to compare the total recoil-ion spectra differential in transverse momenta and recoil-ion charge state, Fig. 8. The theoretical values shown by the lines again have been convoluted with the gas target's Boltzmann temperature distribution to make quantitative comparisons possible. In general, there is reasonable accord between theory and experiment, indicating that the basic underlying physics is being accounted for in the nCTMC calculations. A major difference in absolute magnitude exists for recoil-ion charge state $i=8$, further indicating an overestima-
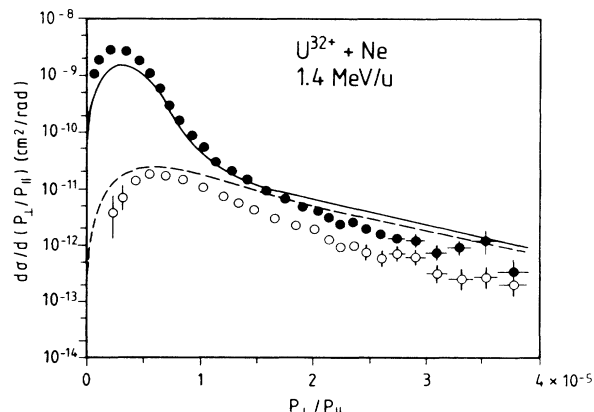

FIG. 7. Differential cross sections for the transverse momentum of the recoil ion $(p_\perp)$ divided by the parallel momentum of the projectile $(p_\parallel)$. The total (ionization plus electron capture) and the single-electron-capture spectra are given by the solid and open circles for the experimental data, and the solid and dashed lines for the nCTMC calculations, respectively. The theoretical values have been folded with the thermal energy distribution of the Ne target.
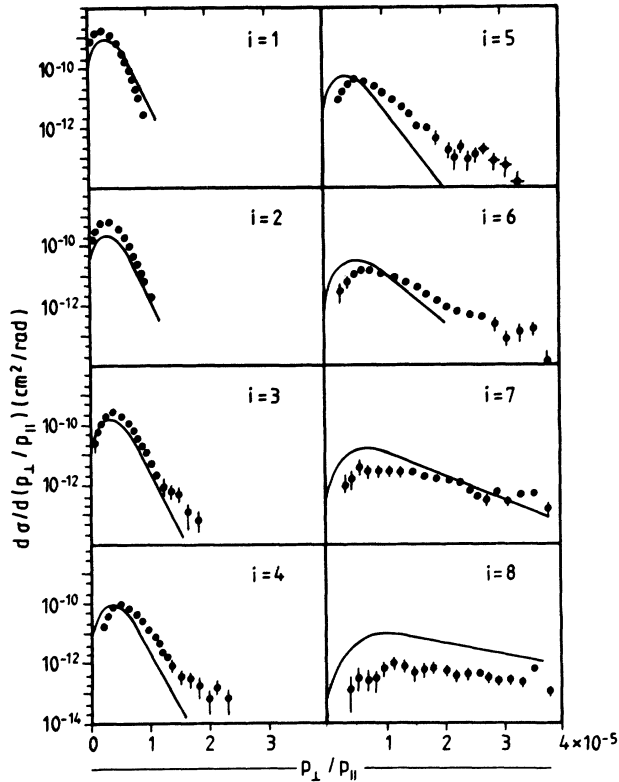
FIG. 8. Same as Fig. 7, except the results are further differential in the Ne^{i+} recoil-ion charge state.

tion of the transition probabilities at small impact parameters, $b \lesssim 2a_0$. In these collisions, it is quite probable that ignoring the electron-shell structure of the U^{32+} ion in the calculations is not a valid assumption. Interpenetration of the projectile's and target's electron shells will yield a time-dependent effective charge for the projectile ion, which will give rise to a general broadening and lowering of the specific recoil-ion charge-state transition probabilities for $b \lesssim 2a_0$ or $i \gtrsim 6$, see Fig. 2. It is also possible that the experimental data are slightly broadened to higher momenta due to secondary charge-exchange collisions of the recoil ions with their parent gas. Due to low gas pressures, this process will be infrequent, but the reactions are highly exothermic, and a gain of momentum will be realized.

As of yet, there is little experimental information as to the angular scattering of the recoil ion. There is one measurement on a low-charge-state-projectile system by Lepera et al.,[39] 0.64-MeV/u Cl^{4+} +Ne, which indicates that the recoil ions may be quite broadly distributed in the 76°–104° angular range. However, within a two-body inelastic-collision picture that ignores anistropic scattering by the ejected electrons, conservation of momentum and energy leads one to expect a forward peaking of the recoil ions to a region between 60° and 80° with no scattering beyond 90°. The shift of the peak depends on the magnitude of the energy loss by the projectile.

Calculated nCTMC values for the recoil-ion angular

scattering, Fig. 9, are in contrast to the two-body picture. In general, we find a slight backward enhancement of the cross sections. Isotropic scattering is realized for the low recoil-ion charge states, with peaked structure only being observed for the high recoil-ion charge states that are produced in small-impact-parameter collisions. Conservation of energy and momentum for both the heavy particles and the electrons is maintained by the nCTMC method when applied to reaction (1). Hence we are lead to an increasing awareness of the possible role of the ejected electrons in the momentum balance between the heavy particles. The relatively high momenta of the electrons, Table I, when combined with their large angle scattering, Figs. 5 and 6, indicate that the sum of the transverse momenta of the ionized electrons is comparable to that of the heavy particles. Moreover, for this effect to be observed, the ejected electrons must be anisotropically emitted during the collision.

To show clearly the effect of the anisotropic ejection of the ionized electrons, calculated differential cross sections are shown in Fig. 10 for the transverse momenta of the projectile and recoil ions relative to the total momentum of the projectile. For the projectile, such a plot is equivalent to the familiar $d\sigma/d\theta$-versus-θ representation. The calculations are also differential in the recoil-ion charge state and have not been masked by Boltzmann averaging over the target atom's initial temperature distribution.

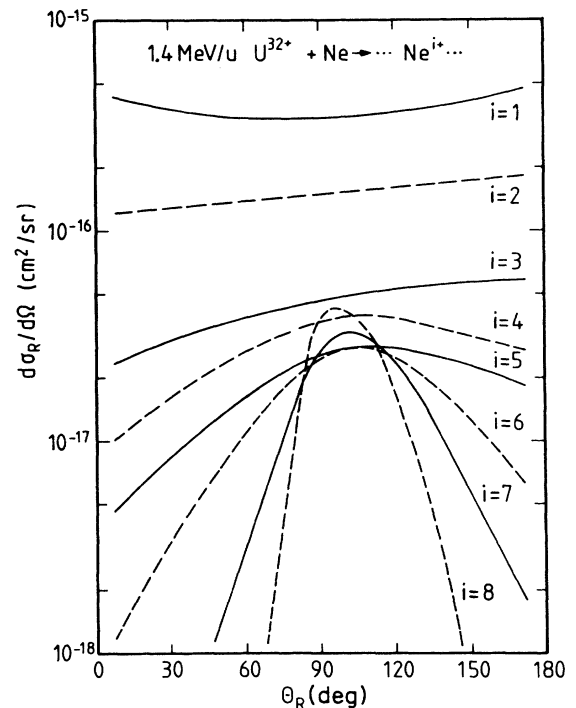If the scattering is considered within a two-body col-

FIG. 9. Calculated differential cross sections for the angular scattering of the recoil ions as a function of the recoil-ion charge state.
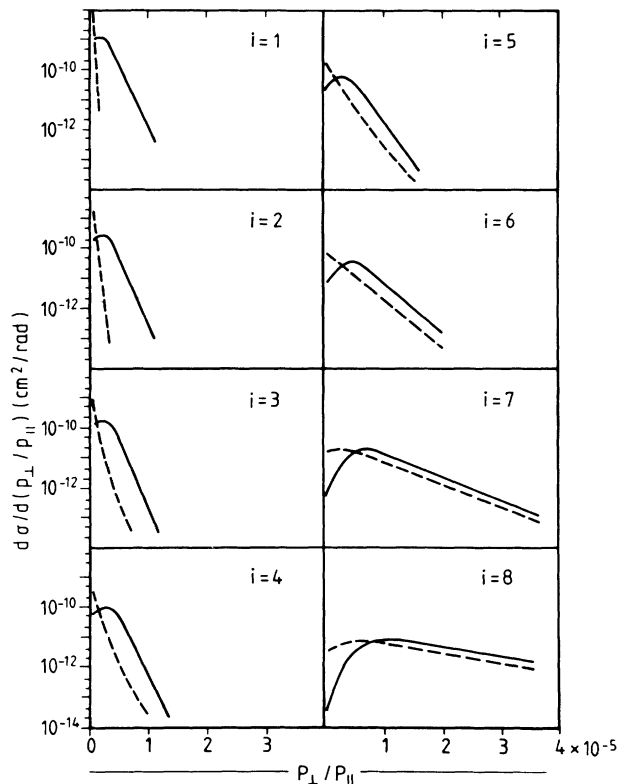
FIG. 10. Calculated differential cross sections for the transverse momentum $(p_\perp)$ of the recoil ion (solid lines) and the projectile (dashed lines) divided by the parallel momentum of the projectile $(p_\parallel)$. The cross sections include both the ionization and electron-capture processes, and have not been averaged for a thermal distribution of target atoms.

lision picture, both the projectile's and recoil ion's differential cross sections would be equal. In fact, we find orders-of-magnitude difference in the cross sections, especially for low recoil-ion charge states. The assumption of two-body scattering is clearly in disagreement with the results presented here. Other calculations[35] have made such an assumption, and have employed a screened Bohr potential to obtain reasonable agreement with the experimental recoil-ion data shown in Fig. 8. However, the calculations are marred by an error in the conversion from center-of-mass to laboratory coordinates. Reanalysis of the calculations leads to theoretical values in general agreement[40] with the projectile-scattering results given in Fig. 10.

From Fig. 10, a general trend emerges indicating that the importance of the electron momenta in the angular scattering manifests itself at impact parameters outside the dimensions of the atomic target. For large impact parameters and low recoil-ion charge-state production, it appears that the main interaction is between the electrons and the recoil-ion nucleus. However, at the opposite extreme, for impact parameters within the target atom's radius, the magnitude of the transverse momenta of the heavy particles is comparable, indicating that the electron transverse momenta are either isotropic or have

magnitudes less than that of the heavy particles.

To explore such ionization mechanisms more completely, we have calculated the total yields of the various collision products in the azimuthal plane perpendicular to the initial direction of the projectile (we shall term it the φ plane). The zero-degree position is determined by the direction of the position vector of the projectile perpendicular to the z axis before the collision (i.e., the impact-parameter direction). Note, the initial momentum of the projectile is in the $+z$ direction. Figure 11 presents the φ dependencies for scattered products differential in the recoil-ion charge state.

As a general observation, we note that the electrons are preferentially scattered to azimuthal angles directed towards the projectile's distance of closest approach, or $\varphi = 0°$. The focusing becomes more diffuse for higher recoil-ion charge states or decreasing impact parameters. For low charge states $i \leq 4$, we find the projectile scattered to negative deflection angles. This is due to two effects. The smaller of the two is from the attractive potential caused by the dipole polarization of the target atom induced by the projectile's point charge on its approach. The second, and most important effect, is due to polarization of the slow (relative to the projectile's velocity) ionized electrons that are associated with continuum levels located between the projectile ion and target nucleus. These relatively slow, anisotropically scattered electrons more than compensate for the repulsive heavy-

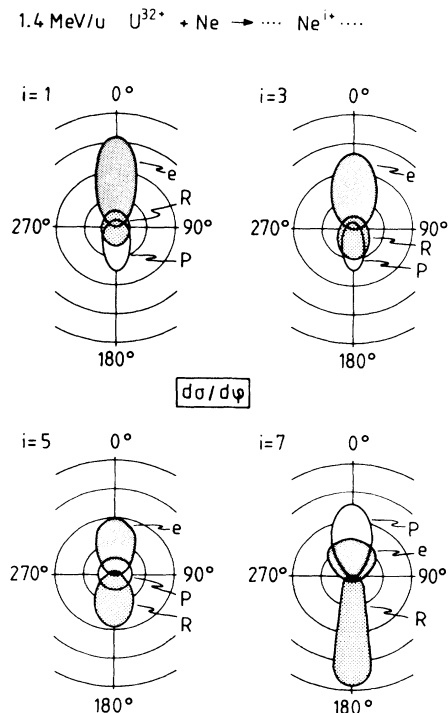1.4 MeV/u U^{32+} + Ne $\longrightarrow$ ···· Ne^{i+} ····

FIG. 11. Calculated yield distributions in the azimuthal plane perpendicular to the projectile's direction. The electron distributions are denoted by the symbol e and a dark mask. The recoil ions are given by R and a light mask, while those for the projectile P have a clear mask.

particle interaction by virtue of their closer proximity to the projectile. We find the negative-angle deflections of the projectile to be limited to $\sim 1 \times 10^{-6}$ rad. The broadening of the scattering to $\varphi \neq 0°$ is due to projectile scattering from the target electrons.

At intermediate-impact parameters, $b \approx 3a_0$, we find nearly zero-angle deflection by the projectile, see the $i = 5$ case of Fig. 11. This is due to near equal cancellation between the attractive polarization potential and the repulsive Coulomb interaction between the final-state heavy nuclei. At small impact parameters such as for Ne^{7+} production, the scattering is dominated by the nuclear-nuclear repulsion. In contrast, the recoil ions are isotropically scattered for large-impact-parameter collisions, and are strongly deflected towards azimuthal angle $\varphi \approx 180°$ only in the hard collisions which lead to high recoil-ion charge states.

Figure 11 indicates that the transverse-momentum balance between products is strongly dependent on the impact parameter. For large impact parameters, the projectile's negative-angle deflection is balanced by the momentum of the ejected electrons. At intermediate impact parameters (near the zero of the deflection function), the ejected-electron transverse momentum balances that of the recoil ion. Only at small impact parameters is the conventional two-body picture realized, with the projectile's transverse momentum being equal and opposite to that of the recoil ion.

There are several implications of the above picture of the ionization dynamics. The first is that the negative-angle deflection of the projectile removes the one-to-one correspondence between scattering angle and impact parameter (in lowest order, there will be three impact parameters corresponding to a given scattering angle). The second result is that the rainbow angle interference structure may be observable even in MeV/u collisions. However, the most important result is that the heavy-particle angular scattering is dominated by the anisotropic ejection of ionized electrons. This leads to the invalidity of applying a central two-body potential to describe the heavy-particle scattering.

Stopping powers

The stopping power $S = dE/dx$ for a system provides a measure of the energy deposited by the projectile during a collision. Stopping-power measurements provide a convenient test of theoretical predictions. Moreover, accurate calculations can provide information as to the partitioning of the energy deposition among the various degrees of freedom such as ionization energies, δ electrons, electron capture, and excitation. We will show that stopping-power measurements primarily probe a small subset of the impact parameters associated with ionization-cross-section measurements, and as such, compliment this latter work.

The results of nCTMC calculations for the 1.4-MeV/u $U^{32+} + Ne$ system are given in Table II. We find that $\sim 55\%$ of the energy deposited resides in the kinetic energy of the δ electrons. Closely related is that $\sim 19\%$ of the energy deposited is given up to the target atom in the

TABLE II. Stopping-power components for 1.4-MeV/u $U^{32+} + Ne$. A similar calculation on 1.4-MeV/u $U^{29+} + Ne$ (the thick-target equilibrium charge state) yields a total stopping power of 3.00×10^{-12} eV/(atom/cm^{-2}). The experimental value (Ref. 41) for this system is 3.16×10^{-12} eV/(atom/cm^2).

Components	Stopping power [eV/(atom/cm^2)]
δ-electrons	1.94×10^{-12}
Ionization	0.68×10^{-12}
Electron capture[a]	0.27×10^{-12}
Excitation	0.63×10^{-12}
Nuclear	$< 10^{-14}$
Total	3.52×10^{-12}

[a]The total stopping power associated with electron-capture events is 1.93×10^{-12} eV/(atom/cm^2). However, this latter value includes major contributions from the high level of δ-electron emission concomitant with electron capture in small-impact-parameter collisions.

sequential binding energies needed to remove multiple electrons to the continuum with zero translational energy relative to the target. An important component of energy loss is from electron capture. Of the total, only $\sim 8\%$ of the energy deposition resides in the removal of electrons from the target to a bound state of the projectile ion. However, if one focuses on the collisions that give rise to single- or multiple-electron capture, their contribution to the total stopping power is $\sim 55\%$. The reason for such a high percentage is that these same collisions also yield high levels of multiple ionization, Fig. 1, and excitation. A significant fraction of the energy loss is associated with excitation of the target ion after the collision, $\sim 18\%$. We expect that this excitation will lead to a large component of uv and x-ray photons since the energy deposition is heavily weighted to small impact parameters where the residual target ion is left in a high stage of multiple ionization.

In Fig. 12 is shown the differential stopping power in terms of the impact parameter of the collision. We find
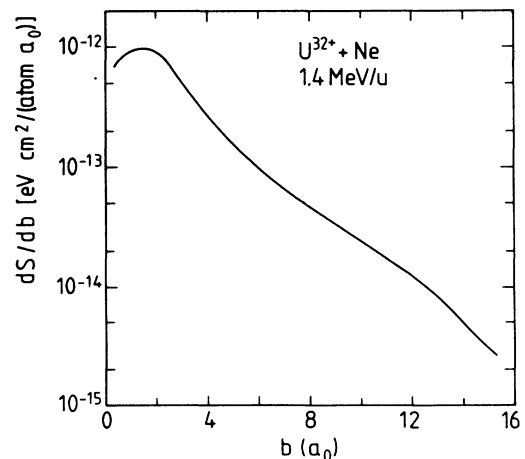

FIG. 12. Calculated stopping-power differential in impact parameter.

that $\sim 84\%$ of the energy loss occurs at impact parameters $b \leq 4a_0$. This implies that a major fraction of the projectile's energy loss is expended in ionizing the target atom to charge states $i \gtrsim 4$ (Fig. 2), and in the production of energetic electrons (Table I). Also, the photon emission will be strongly connected to the high recoil-ion charge states.

A direct comparison to experiment for the 1.4-MeV/u U^{32+} + Ne calculated stopping power is not available. However, equilibrium U^{q+} charge-state measurements have been made by Geissel et al.[41] At 1.4 MeV/u in neon, the equilibrium charge is U^{29+}, and the measured stopping power is 3.16×10^{-12} eV/(atom/cm^2). A calculation by us for U^{29+} yields 3.00×10^{-12} eV/(atom/cm^2) which should be considered very reasonable agreement for a direct calculation of the stopping power for an energetic, heavy-ion system.

SUMMARY

Extensive calculations and measurements have been presented for the angular scattering of the heavy particles and electrons in the prototype energetic, heavy-ion 1.4-MeV/u U^{32+} + Ne collision system. In general, good agreement is realized between theoretical nCTMC calculations and experimental results. Disagreements primarily occur for small-impact-parameter collisions where there is penetration of the target atom's electron cloud by the projectile ion. For such collisions, it appears that in the future it will be necessary to include the electronic levels of the projectile to accurately account for decreased screening of the projectile's nuclear charge.

The classical nCTMC calculations have allowed us, for the first time, to follow the collision dynamics of all the scattered particles during the collision. Energy and angular studies reveal a high degree of anisotropy in the ejected-electron emission. This asymmetry leads to an unexpected importance of the electrons' dynamics in determining the transverse-momentum distributions of the heavy-projectile and target-recoil ions. Negative-angle deflections of the projectile ion are found which lead to a nonuniqueness in the relationship between scattering angle and impact parameter for a major fraction of the ionizing collisions. The use of a simple two-body picture to describe the angular differential cross sections for the recoil and projectile ions is found to be invalid. A central conclusion of our work is that the anisotropic δ-electron emission invalidates the use of a spherically symmetric potential to describe detailed collision dynamics of multielectron transitions such as those given by reaction (1). Exception to this conclusion occurs only at small impact parameters where the electrons are scattered isotropically.

Projectile energy-loss calculations are found to be in good agreement with observations. The calculations indicate the relative importance of small-impact-parameter collisions in the determination of stopping powers. Furthermore, target excitation, which will lead to uv and x-ray photon emission, appears to be an important component to energy loss in energetic, heavy-ion collisions.

ACKNOWLEDGMENTS

[1]J. R. Mowat, I. A. Sellin, D. J. Pegg, R. S. Peterson, J. R. Macdonald, and M. D. Brown, Phys. Rev. Lett. **30**, 1289 (1973).

[2]R. Mann, F. Folkmann, and K. O. Groeneveld, Phys. Rev. Lett. **37**, 1674 (1976).

[3]C. L. Cocke, Phys. Rev. A **20**, 749 (1979).

[4]A. S. Schlachter, K. H. Berkner, W. G. Graham, R. V. Pyle, P. J. Schneider, K. R. Stalder, J. W. Stearns, J. A. Tanis, and R. E. Olson, Phys. Rev. A **23**, 2331 (1981).

[5]S. Kelbch, J. Ullrich, R. Mann, P. Richard, and H. Schmidt-Böcking, J. Phys. B **18**, 323 (1985).

[6]A. Müller, B. Schuch, W. Groh, E. Salzborn, H. F. Beyer, P. H. Molker, and R. E. Olson, Phys. Rev. A **33**, 3010 (1986).

[7]T. J. Gray, C. L. Cocke, and E. Justiniano, Phys. Rev. A **22**, 849 (1986).

[8]J. C. Levin, R. T. Short, S. C. O, H. Cederquist, S. B. Elston, J. P. Gibbons, I. A. Sellin, and H. Schmidt-Böcking, Phys. Rev. A **36**, 1649 (1987).

[9]R. E. Olson, J. Ullrich, and H. Schmidt-Böcking, J. Phys. B **20**, L809 (1987).

[10]G. P. Grandrin, D. Hennecart, X. Husson, D. Lecler, I. Lesteven-Vaisse, and D. Lisfi, Europhys. Lett. **6**, 683 (1988).

[11]R. Schuch, H. Schöne, P. D. Miller, H. F. Krause, P. F. Dittner, S. Datz, and R. E. Olson, Phys. Rev. Lett. **60**, 925 (1988).

[12]S. Kelbch, C. L. Cocke, S. Hagmann, M. Horbatsch, C. Kelbch, R. Koch, and H. Schmidt-Böcking, Phys. Lett. A **127**, 92 (1988).

[13]C. Kelbch, R. E. Olson, S. Schmidt, H. Schmidt-Böcking, and S. Hagmann, J. Phys. B (to be published).

[14]M. Gryzinski, Phys. Rev. A **138**, 336 (1965).

[15]J. M. Hansteen, A. M. Johansen, and L. Kocbach, At. Data Nucl. Data Tables **15**, 305 (1975).

[16]R. E. Olson, J. Phys. B **12**, 1843 (1979).

[17]R. E. Olson and A. Salop, Phys. Rev. A **16**, 531 (1977).

[18]J. M. Hansteen and O. P. Mosebekk, Phys. Rev. Lett. **29**, 1361 (1972).

[19]J. H. McGuire and L. Weaver, Phys. Rev. A **16**, 41 (1977).

[20]A. Russek and J. Meli, Physica **46**, 222 (1970).

[21]Q. C. Kessel and E. Everhart, Phys. Rev. **146**, 16 (1966).

[22]E. Everhart and Q. C. Kessel, Phys. Rev. **146**, 27 (1966).

[23]R. E. Olson, in Electronic and Atomic Collisions, edited by H. B. Gilbody, W. R. Newell, F. H. Read, and A. C. H. Smith (Elsevier Science, New York, 1988), pp. 271–285.

[24]M. Horbatsch and R. M. Dreizler, Phys. Lett. **113A**, 251

(1985).

[25]M. Horbatsch and R. M. Dreizler, Z. Phys. D **2**, 183 (1986).

[26]J. H. McGuire, Phys. Rev. A **36**, 1114 (1987).

[27]J. F. Reading and A. L. Ford, Phys. Rev. Lett. **58**, 543 (1987).

[28]R. E. Olson, Phys. Rev. A **36**, 1519 (1987).

[29]R. L. Becker and A. D. MacKellar, J. Phys. B **17**, 3923 (1984).

[30]R. E. Olson, Phys. Rev. A **24**, 1726 (1981).

[31]R. C. Isler and R. E. Olson, Phys. Rev. A **37**, 3399 (1988).

[32]H. Berg, R. Dörner, C. Kelbch, S. Kelbch, J. Ullrich, S. Hagmann, P. Richard, H. Schmidt-Böcking, A. S. Schlachter, M. Prior, H. J. Crawford, J. M. Engelage, I. Flores, D. H. Loyd, J. Pedersen, and R. E. Olson, J. Phys. B **21**, 3929 (1988).

[33]J. Ullrich and H. Schmidt-Böcking, Phys. Lett. **125A**, 193 (1988).

[34]J. Ullrich, H. Schmidt-Böcking, and C. Kelbch, Nucl. In-

strum. Methods A **268**, 216 (1988).

[35]J. Ullrich, M. Horbatsch, V. Dangendorf, S. Kelbch, and H. Schmidt-Böcking, J. Phys. B **21**, 611 (1988).

[36]J. Ullrich, R. E. Olson, R. Dörner, V. Dangendorf, S. Kelbch, H. Berg, and H. Schmidt-Böcking, J. Phys. B **22**, 627 (1989).

[37]M. Horbatsch, Z. Phys. D **1**, 337 (1986).

[38]W. Erb, Gesellschaft für Schwerionenforschung, Darmstadt Report No. P-7-78, 1978 (unpublished).

[39]C. E. Gonzalez Lepera, M. Breinig, J. Burgdörfer, R. DeSerio, S. B. Elston, J. P. Gibbons, H-P Hülskötter, L. Liljeby, R. T. Short, and C. R. Vane, Nucl. Instrum. Methods, B **24/25**, 316 (1987).

[40]M. Horbatsch (private communication).

[41]H. Geissel, Y. Laichter, W. F. W. Schneider, and P. Armbruster, Nucl. Instrum. Methods **194**, 21 (1982).